Computational fluid dynamics analysis of the hydraulic (filtration) efficiency of a residential swimming pool

J. Zhang, N. Sinha, M. Ross and A. E. Tejada-Martínez

ABSTRACT

Hydraulic or filtration efficiency of residential swimming pools, quantified in terms of residence time characteristics, is critical to disinfection and thus important to public health. In this study, a three-dimensional computational fluid dynamics model together with Eulerian and Lagrangian-based techniques are used for investigating the residence time characteristics of a passive tracer and particles in the water, representative of chemicals and pathogens, respectively. The flow pattern in the pool is found to be characterized by dead zone regions where water constituents may be retained for extended periods of times, thereby potentially decreasing the pool hydraulic efficiency. Two return-jet configurations are studied in order to understand the effect of return-jet location and intensity on the hydraulic efficiency of the pool. A two-jet configuration is found to perform on par with a three-jet configuration in removing dissolved constituents but the former is more efficient than the latter in removing or flushing particles. The latter result suggests that return-jet location and associated flow circulation pattern have an important impact on hydraulic efficiency. Thus return-jet configuration should be incorporated as a key parameter in the design of swimming pools complementing current design standards.

Key words | computational fluid dynamics, hydraulic efficiency, swimming pools

J. Zhang
N. Sinha
M. Ross
A. E. Tejada-Martínez (corresponding author)
Department of Civil and Environmental Engineering,
University of South Florida,
4202 E. Fowler Ave, Tampa, FL 33620,
USA
E-mail: *aetejada@usf.edu*

J. Zhang
Carollo Engineers, Inc.,
1218 Third Ave, Suite 1600, Seattle, WA 98101,
USA

INTRODUCTION

Although water disinfection processes in swimming pools and baffled ozone contactors function in a similar fashion (Caro & Gallego 2007), the hydraulic efficiency of residential and public swimming pools has received minimal attention compared to the hydraulic efficiency of ozone contactors. Hydraulic efficiency is an important component of the water disinfection process via chlorination or ozonation, considering the potential carcinogenic products formed in this process. Water treated by chlorine species or ozone may lead to undesired by-products such as chlorite, chlorate and bromate, which are responsible for adverse effects on human health (Beech *et al.* 1980; Michalski & Mathews 2007; Zwiener *et al.* 2007). For example, according to Zwiener *et al.* (2007), swimming or showering with chlorinated water has been linked to a 1.6–2 increased risk factor for bladder cancer. As noted by Zwiener *et al.* (2007) a major issue in pool water treatment is to ensure sufficient disinfection while minimizing disinfection by-products. Improving the hydraulic efficiency of a pool would allow for a smaller dose of disinfectant to be used, thus reducing the formation of harmful disinfection by-products.

Continued advances in computational power have enabled accurate computational fluid dynamics (CFD)-based analysis of the flow in baffled ozone reactors (e.g. Henry & Freeman 1995; Cockx *et al.* 1999; Do-Quang *et al.* 1999; Huang *et al.* 2002, 2004; Zhang *et al.* 2007, 2013, 2014a, 2016) resulting in the identification of localized flow phenomena such as re-circulation zones or 'dead zones'

doi: 10.2166/wh.2018.110

which serve to hinder disinfection efficiency. In recent years similar localized flow phenomena have also been identified in swimming pools by CFD analysis (Cloteaux *et al.* 2013; Lewis *et al.* 2015), indicating that the methods in the current PWTAG guidance (PWTAG 2009) may not be suitable to calculate the turnover time. Furthermore, CFD was also used to study the retention time of chemicals and pathogens in swimming pools via tracer studies (Cloteaux *et al.* 2013; Lewis *et al.* 2015). In these simulations, the tracer studies were based on an Eulerian approach (Zhang *et al.* 2014b). This approach enables tracking of dissolved chemicals but is not able to capture the behavior of suspended solids (e.g. pathogens). In the present study we explore Eulerian and Lagrangian approaches in investigating the transport of dissolved agents and suspended particles in a typical swimming pool configuration. The Lagrangian approach facilitates tracking of the particles. In particular we study how the return-jet configuration of the pool affects the hydraulic or filtration efficiency through residence time characteristics of water constituents. The size of particles studied is consistent with the typical size of bacteria such as *Escherichia coli* and *Salmonella*, which are commonly found in swimming pools.

Biofilms allow for the collection of bacteria which is one of the major problems in swimming pools. Dead zones are known as the 'birthing grounds' for biofilms. The bottom half of the pool, especially in pools without main or bottom drains, and the corners of rectangular pools are likely dead zones. The Lagrangian particle tracking results in the present study suggest that it should be possible to design the return-jet configuration of the pool to help minimize these dead zones and thus reduce biofilm formation.

GOVERNING EQUATIONS

The present study makes use of the frozen flow strategy employed in other similar studies of water disinfection systems (e.g. see Zhang *et al.* 2014b). That is, assuming steady flow, the mean flow is first computed followed by Eulerian and Lagrangian studies of hydraulic efficiency making use of the mean flow solution. In this section the flow governing equations and the Eulerian and Lagrangian approaches to quantify hydraulic efficiency are introduced sequentially.

Flow governing equations

The governing flow equations consist of the incompressible steady-state Reynolds-averaged continuity and Navier–Stokes (RANS) equations:

$$\frac{\partial \langle u_i \rangle}{\partial x_i} = 0 \tag{1}$$

$$\langle u_j \rangle \frac{\partial \langle u_i \rangle}{\partial x_j} = -\frac{1}{\rho}\frac{\partial \langle p \rangle}{\partial x_i} + \nu \frac{\partial^2 \langle u_i \rangle}{\partial x_j^2} - \frac{\partial \langle u'_i u'_j \rangle}{\partial x_j} \tag{2}$$

where brackets denote Reynolds averaging and $\langle u_i \rangle$ is the ith component of the Reynolds-averaged or mean velocity; ρ is the constant water density; $\langle p \rangle$ is the mean pressure; ν is molecular kinematic viscosity; x_i is the coordinate in the ith direction. The Reynolds stress tensor $-\langle u'_i u'_j \rangle$ (defined in terms of velocity fluctuation u'_i) is closed using an eddy viscosity model (namely the classical k-ε model) in which:

$$-\langle u'_i u'_j \rangle = \nu_t \frac{\partial \langle u_i \rangle}{\partial x_j} \tag{3}$$

and the eddy viscosity is:

$$\nu_t = C_\mu \frac{k^2}{\varepsilon} \tag{4}$$

where k is the turbulent kinetic energy, ε is turbulent kinetic energy dissipation and $C_\mu = 0.09$. Spatial distributions of k and ε are specified via transport equations part of the standard k-ε model (Wilcox 1994) equipped with standard wall functions (Launder & Spalding 1974).

Eulerian passive tracer transport

Eulerian passive tracer transport studies will be based on the unsteady Reynolds-averaged advection-diffusion equation for tracer concentration:

$$\frac{\partial \langle C \rangle}{\partial t} + \langle u_j \rangle \frac{\partial \langle C \rangle}{\partial x_j} = -\frac{\partial \langle u'_i C' \rangle}{\partial x_j} \tag{5}$$

where $\langle C \rangle$ is the Reynolds-averaged tracer concentration and $\langle u_j \rangle$ is the Reynolds-averaged steady state flow solution. The tracer is representative of a non-reacting dissolved

species in the water. The turbulent tracer concentration flux $-\langle u_j' C' \rangle$ is modeled as:

$$-\langle u_i' C' \rangle = D_t \frac{\partial \langle C \rangle}{\partial x_j} \tag{6}$$

Note that $\langle C \rangle$ is time-dependent due to its transient boundary conditions described further below. The eddy (turbulent) diffusivity is taken as $D_t = \nu_t / Sc_t$ where eddy viscosity ν_t is computed as described earlier and the turbulent Schmidt number, Sc_t, is taken as 0.7 (Launder 1978). In Equation (5), molecular diffusion has been neglected as it is much less than turbulent diffusion throughout the flow domain.

Two types of studies were conducted using the Eulerian approach previously described. In the first type, referred to as *tracer pulse studies*, a pulse or slug of the tracer was released through the pool return-jets at the beginning of the simulation and extending over a time period equal to 2% of the theoretical residence time. In these studies the tracer concentration at the flow outlet (i.e. the skimmer) was tracked over time in order to generate residence time distributions useful for quantifying the residence time characteristics of the pool. In the second type of Eulerian-based studies, referred to as the *volume flushing studies*, the pool was initially filled with tracer which was flushed out over time as fresh (tracer-free) water was discharged from the return-jets. Tracer concentration averaged over the pool volume was tracked over time in order to quantify the flushing behavior of the pool.

Solution of the flow equations and tracer transport equation were conducted via standard finite volume discretization techniques implemented within the well-known ANSYS Fluent software (2006).

Lagrangian particle tracking

The Lagrangian discrete phase model in ANSYS Fluent follows the Euler–Lagrange approach. The fluid phase is treated as a continuum by solving the Navier–Stokes equations as described earlier, while the dispersed phase is solved by tracking individual particles through the calculated flow field. In the Lagrangian discrete phase model, the trajectory of a discrete phase particle is predicted by integrating the force balance on each particle, which is written in a Lagrangian reference frame. This force balance equates the particle inertia with the forces acting on the particle, and can be written as:

$$\frac{d\boldsymbol{u}_p}{dt} = F_D(\boldsymbol{u} - \boldsymbol{u}_p) \tag{7}$$

where the fluid and particle densities have been assumed to be the same, $\boldsymbol{u}$ is the fluid phase velocity defined as $\langle \boldsymbol{u} \rangle + \boldsymbol{u}'$ with $\langle \boldsymbol{u} \rangle$ the mean velocity obtained from solution of the RANS equations described earlier and $\boldsymbol{u}'$ the turbulent fluctuation to be defined further below, $\boldsymbol{u}_p$ is the particle velocity, and $F_D(\boldsymbol{u} - \boldsymbol{u}_p)$ is the drag force per unit particle mass with:

$$F_D = \frac{18\mu}{\rho_p d_p^2} \frac{C_D Re}{24} \tag{8}$$

Here, μ is the molecular viscosity of the fluid, ρ_p is the particle density, d_p is the particle diameter, C_D is the drag coefficient which is estimated by the model given in Morsi & Alexander (1972), and Re is the relative Reynolds number which is defined as:

$$Re = \frac{\rho_p d_p |\boldsymbol{u} - \boldsymbol{u}_p|}{\mu} \tag{9}$$

The Cartesian components of the velocity fluctuation $\boldsymbol{u}' = (u'_1, u'_2, u'_2)$ are defined through a random walk model as $u'_1 = u'_2 = u'_2 = \xi\sqrt{2k/3}$, where ξ is a normally distributed random number and k is the turbulent kinetic energy obtained from the k-ε turbulence model described earlier.

In this study, hydraulic efficiency was measured by tracking 100 small neutrally buoyant particles initially distributed throughout the surface of the pool. The size of particles is uniformly 1 micrometer, representing the typical size of bacteria, such as *E. coli* and *Salmonella*, which can sometimes be found in swimming pools.

THE POOL SYSTEM AND NUMERICAL SETTING

Pool drain systems gather a series of components that work in conjunction to distribute and flush the water inside the

pool. This movement of water is typically done by a motor pump, which forces water into the pool via the return-jets. As this occurs, water flows out of the basin through the main drains and the skimmers. These components induce complex three-dimensional circulation patterns that can be characterized by dead zone regions in which water is retained for extended periods of time, ultimately reducing the hydraulic efficiency of the pool.

In this study, two model residential pool configurations were chosen based on realistic specifications in terms of physical size. Specifically, both models, as shown in Figure 1, consist of a rectangular shape 9.8 m long and 4.9 m wide and a variable water depth ranging from 1.2 to 1.8 m for a volume of 19,000 gallons. Dimensions for the skimmer or outflow are 20.32 by 13.97 cm with the water level reaching 7.62 cm along the skimmer height. Return-jets or inflows have circular cross sections, each having a 1.88-cm diameter. Additional relevant dimensions are shown in the schematic in Figure 2. Two return-jet configurations were investigated, shown in Figure 1. Model A is comprised of three return-jets, denoted as jets one, two and three in Figure 1(a). Model B is comprised of two return-jets shown in Figure 1(b). Note that model B consists of return-jets one and three from model A with jet two closed. For simplicity, so as to not create an undesired strong vortex, the models do not contain a bottom drain. However, note that exclusion of drains is not unrealistic as this practice has been trending in the pool industry for safety reasons (Taylor 2015).

In order to compute the flow inside the pool, the volume of the pool geometry was discretized using a variable-size mesh (grid) consisting of 1,619,049 cells or elements (see Figure 3). Element shape varies between hexahedral, tetrahedral and pyramid. To ensure satisfaction of conservation of momentum and mass, the mesh is refined in critical areas where velocities tend to be higher than elsewhere and where openings are on the order of centimeters or less. For example, the mesh resolution is ~1 cm at the skimmer and ~0.02 cm at the return-jets.

The water surface was treated as a no-penetration, zero-shear, rigid lid allowing slip. The total flow rate of return-jets was 25 gpm or 1.578×10^{-3} m^3/s, corresponding to a theoretical residence time (pool volume divided by flow rate) of 12.7 hours. As noted earlier, we considered two models with two and three return-jets, respectively (see Figure 1). Thus the flow rates applied to each return-jet would be the total flow rate divided by two and three for the two models respectively. Atmospheric pressure was imposed at the flow outlet or skimmer. No-slip conditions were imposed at the bottom and side walls of the pool. The mesh described above is such that viscous wall regions (buffer and viscous sub-layers) were not resolved and were instead modeled using a standard wall function (Launder & Spalding 1974). In the numerical tracer studies, at the outlet (i.e. skimmer) and at the walls, the normal gradients of tracer concentration were set to zero (zero-gradient boundary condition) indicating zero diffusive flux across these boundaries. For the tracer pulse studies, in which the tracer concentration

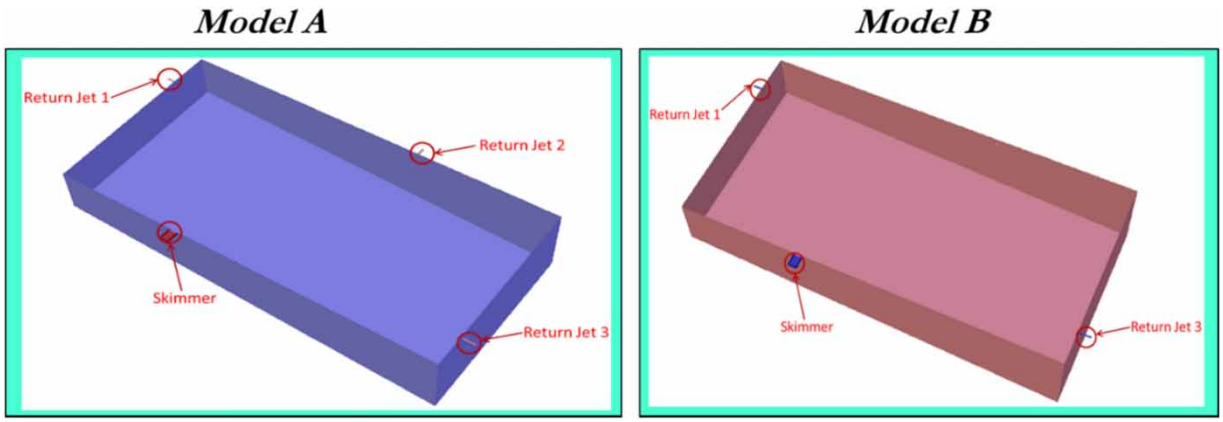

Figure 1 | Model A showing three return-jets and model B showing two return-jets. In both models the pool dimension is 10 m long and 5 m wide, and depth varies between 1.2 and 1.8 m. Both pools hold 19,000 gallons (86,476 L).

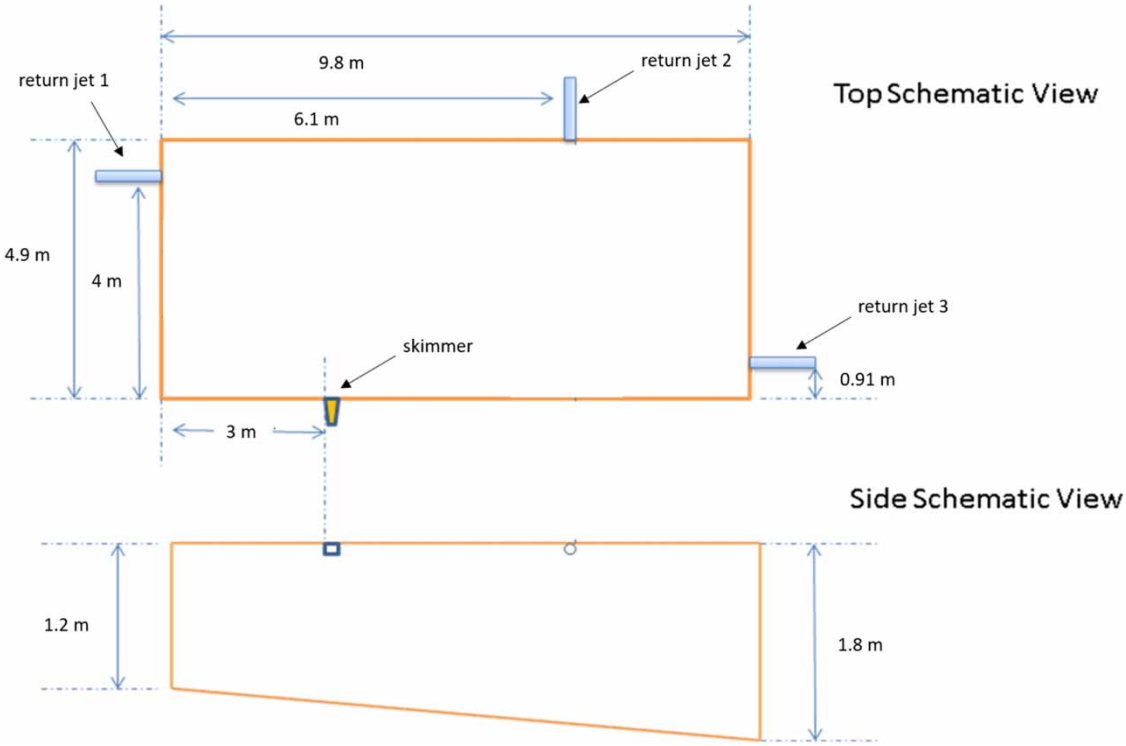

Figure 2 | Top and side schematics of pool model.

was initially set to zero everywhere in the pool, a fixed unit tracer concentration ($C = 1$ mol/L) was set at the return-jets for the first 200–300 seconds of the simulation (less than 1% of the theoretical residence time) followed by setting the concentration to zero at the jets throughout the remainder of the simulation. In the case of the volume flushing studies, in which unit tracer concentration was set everywhere inside the pool volume as the initial condition, zero tracer concentration was set at the return-jets throughout the entire simulation. Thus the water entering through the return-jets was tracer-free and this fresh water eventually displaced or flushed out the tracer initially set within the pool.

RESULTS AND DISCUSSION

In this section, visualizations of the flow patterns in the two swimming pool models are firstly presented. Results from tracer transport and particle tracking are then analyzed to evaluate the hydraulic performance of the two models.

Flow fields

In Figure 4, panels (a) and (b) show the absolute velocity (i.e. speed) at the water surface. The flow patterns are characterized by high-speed core jets or short-circuiting. In model B (Figure 4(b)), two strong jets occupy most of the space near the water surface; in model A (Figure 4(a)) the three jets are relatively weaker partially due to a lower flow rate (the interactions among the three jets can weaken the jets as well), resulting in a large slower-speed region in the middle of the pool.

To further analyze the flow fields, streamlines in both models are plotted in Figure 5. Both flows exhibit complex three-dimensional circulation patterns. Near the surface, the two return-jets model (model B) is characterized by two major circulation zones, both having streamlines passing through the skimmer. Near the surface, the three-jet model (model A) is also characterized by two major zones: a large circulation zone that spans the length of the pool with a smaller zone embedded in the center towards the upper right corner. As seen in Figure 5, panels (a)

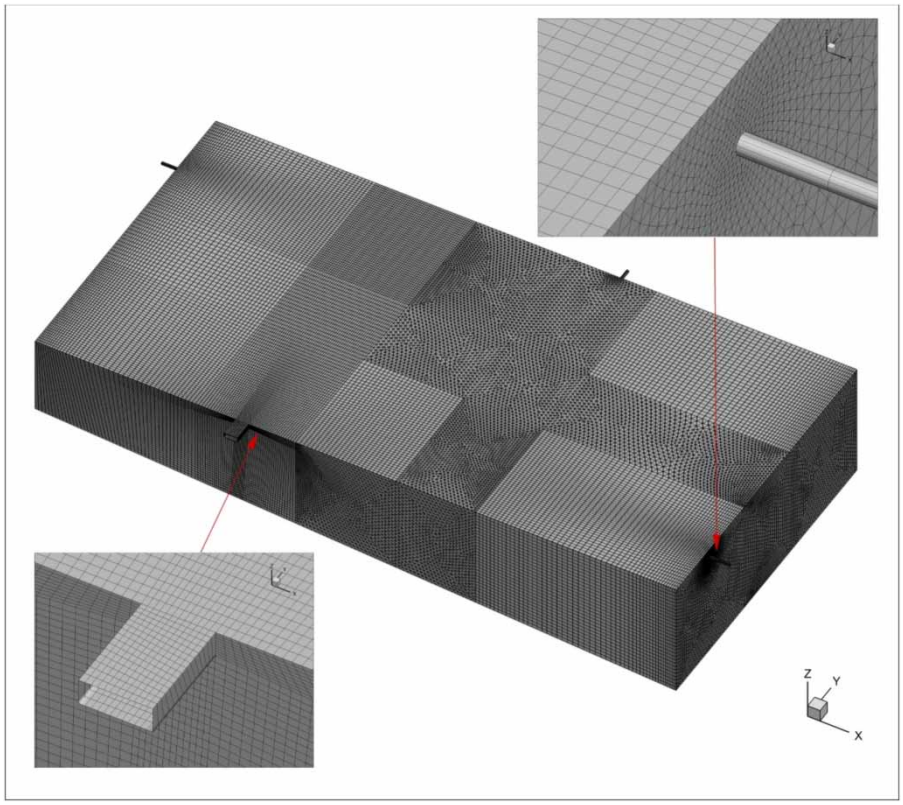

Figure 3 | Discretized geometry with mesh consisting of 1,619,049 elements.

and (b), this embedded circulation zone is isolated because its path-lines do not pass near the skimmer but rather submerge to depths below the skimmer, which contributes to the longer flushing times of particles emanating from this zone (as will be seen through the Lagrangian particle tracking studies presented further below).

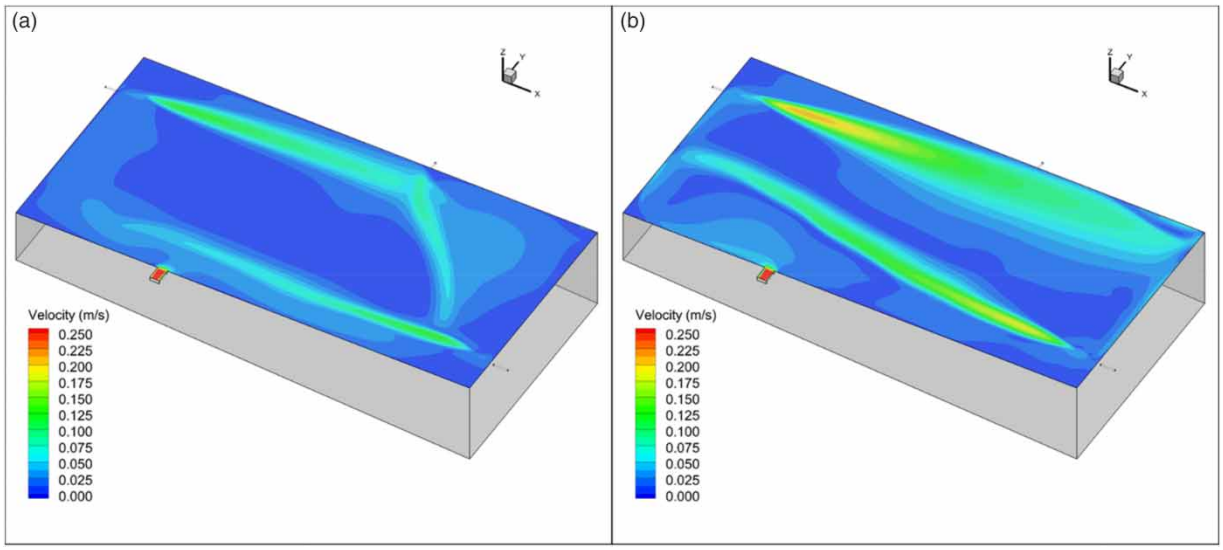

Figure 4 | Surface speed contours in the pool with (a) three jets (model A) and (b) two jets (model B). Velocity units are m/s.

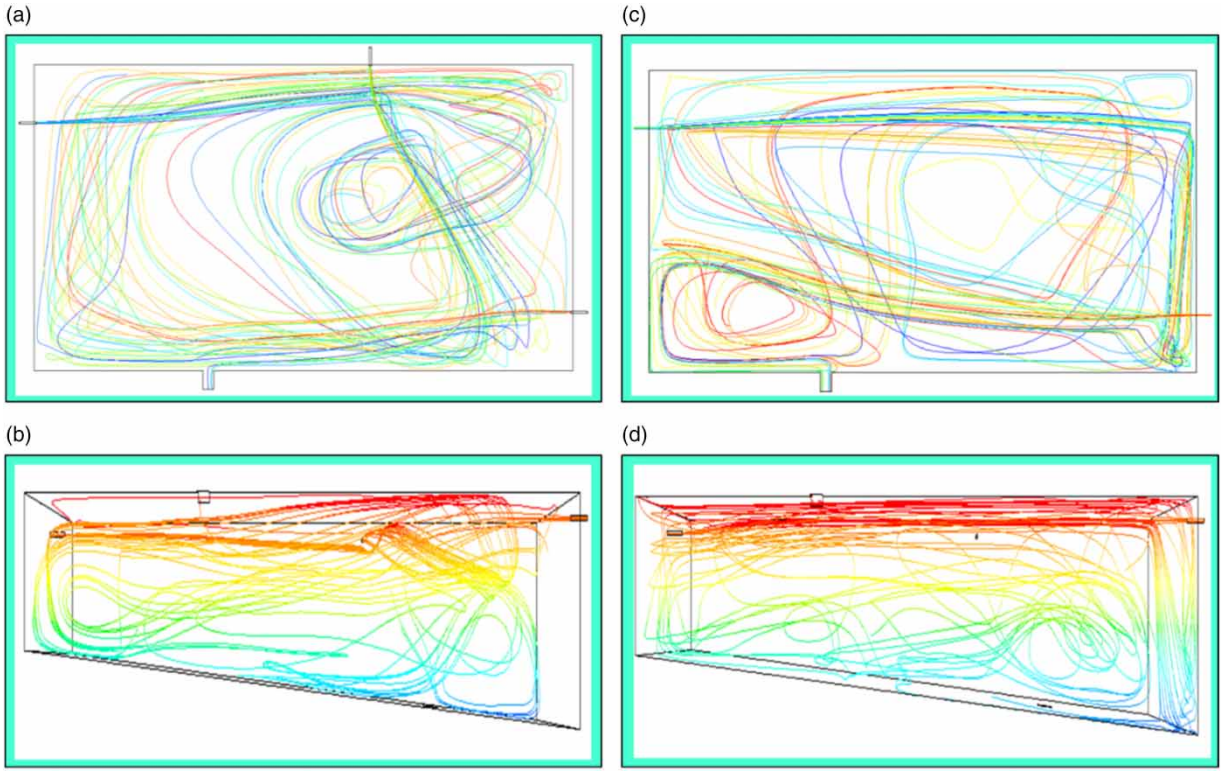

Figure 5 | Top views (a, c) and side views (b, d) of computed fluid particle path-lines in model A (a, b) and model B (c, d). *Note:* the color corresponds to the return-jet from where the pathlines are emanating. Please refer to the online version of this paper to see this figure in color: http://dx.doi.org/10.2166/wh.2018.110.

Eulerian passive tracer transport

In the tracer pulse tests, we considered three scenarios for releasing the tracer: (1) release at return-jet one only; (2) release at return-jet three only; and (3) release at both jets one and three. Figure 6 shows time series of the normalized tracer concentration at the skimmer for all of these scenarios. Note that the tracer concentration is normalized

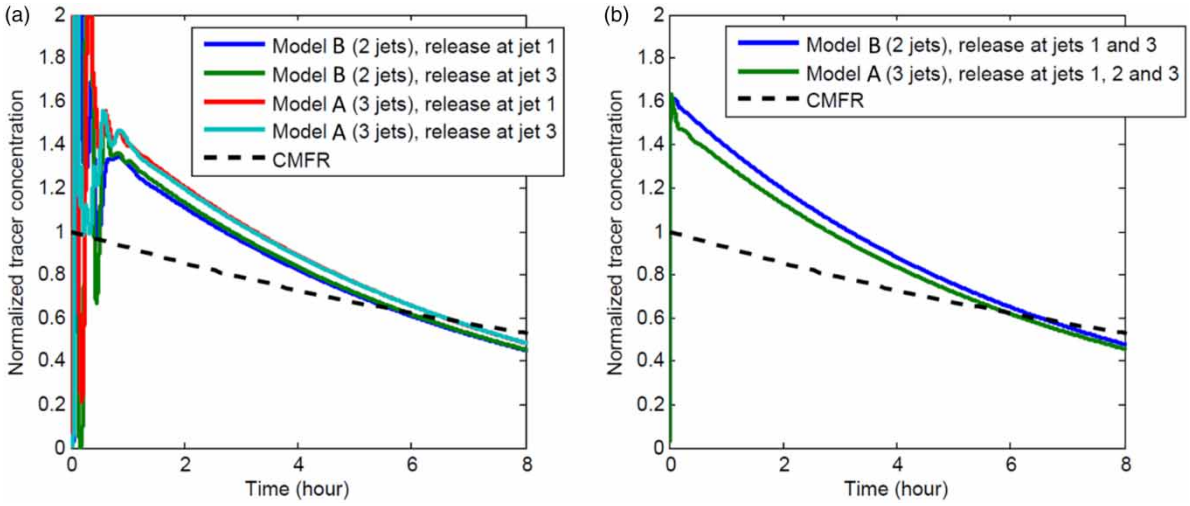

Figure 6 | RTD in model A (three jets) and B (two jets) with tracer released at (a) return-jet one or three and at (b) both return-jets one and three.

by an adjusted initial concentration (calculated as the initial concentration multiplied by the time duration of the tracer release and flow rate and divided by the total volume of the pool). The normalized curve is often referred to as the residence time distribution (RTD). The RTD curves in Figure 6 shows that after 1 hour of the tracer release, the tracer concentration measured at the skimmer decays at nearly the same rate in all cases. After the first hour of tracer release, the spreading of the tracer throughout the pool is controlled by turbulent diffusion which is nearly the same for all scenarios simulated, resulting in the nearly identical tracer concentration decay at the skimmer in all these cases. Furthermore, Figure 6 shows that the tracer concentration decay rate in the scenarios considered is greater than that in a completed mixed flow reactor (CMFR), indicating that the pool may not be assumed to be completely mixed. As the tracer in the scenarios simulated becomes trapped within dead zones, the tracer concentration measured at the skimmer decays at a faster rate than in the CMFR case. Furthermore, note that within the first hour of the tracer release, the spreading of the tracer in the pool is governed by advection and thus short-circuiting effects. This gives rise to the differences in tracer concentration measured at the skimmer within the first hour observed in Figure 6, given the different advection patterns in the various scenarios simulated as described earlier through Figure 5.

To further investigate the hydraulic efficiency of the pool, volume flushing studies were conducted for both models. Recall that in these studies the pool is initially filled with tracer with uniform (homogeneous) concentration. Fresh water (with tracer concentration equal to zero) is then continuously released from the return-jets and the decreasing mass of tracer in the pool is tracked over time. For example, Figure 7 shows a snapshot of normalized tracer concentration contours on the pool surface at $t = 13.4$ hours after fresh water had been flowing into the pool. In model A, there is a greater tracer residual in the center of the pool relative to model B, consistent with the slower moving fluid in the same region seen in the flow speed contours in Figure 4. Although the flow path-lines induced by the different return-jet configurations lead to differences in locations where the tracer tends to remain longer before it is eventually flushed out, the continuous decay of total tracer mass is nearly identical in both models. This can be observed in Figure 8 showing the normalized volume-averaged tracer concentration in the pool as a function of time. Note that the tracer concentrations shown in Figures 7 and 8 have been normalized by the initial uniform tracer concentration in the pool.

Figure 8 also shows the flushing behavior of a CMFR. In the case of the CMFR, there are no dead zones nor associated short-circuiting as the tracer is continuously and vigorously mixed uniformly throughout the entire domain. Meanwhile, in the pool scenarios investigated, short-circuiting provides an avenue for the tracer to initially exit the pool at a faster rate than in the CMFR. However over time, at approximately 5 hours after the fresh water started to be released into the pool, turbulent diffusion becomes dominant over advection (i.e. short-circuiting) and the tracer flushing rate in the pool scenarios begins to approximate the CMFR flushing rate.

Note that although the change of mean tracer residue in the pool cannot be described by the CMFR model, it can still be described by a general exponential model which may be written as:

$$C^n = e^{-A\theta} \tag{10}$$

where C^n is the normalized tracer concentration described above, θ is normalized time (time divided by theoretical residence time), and A is a constant to determined. For the CMFR model, A is 1.0. The value $A = 1.95$ leads to excellent agreement with the simulations (see Figure 8). Thus, the general exponential model with fitted constant can well represent the pool scenarios investigated. Future studies should investigate the robustness of the value of A across a wider variety of pool designs.

Lagrangian particle tracking

One-hundred small (1 micrometer-sized) neutrally buoyant particles initially distributed uniformly on the surface of the pool were tracked using the Lagrangian method described earlier. Figure 9 shows the number of particles flushed out of the pool through the skimmer as a function of time. Pool model B (two-jet configuration) flushes 50%

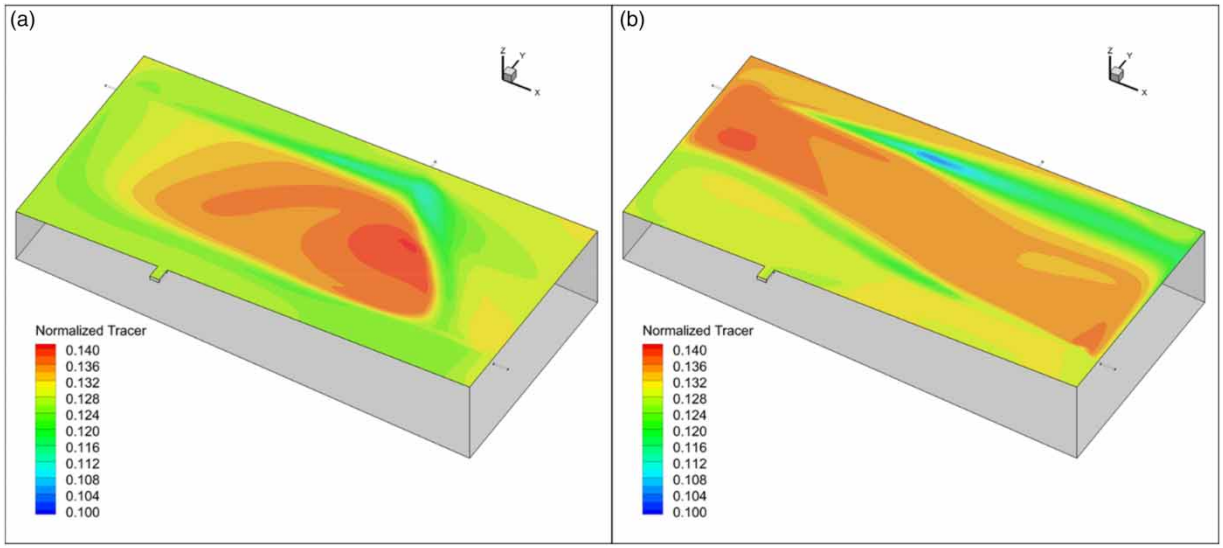

Figure 7 | Tracer residue distribution in the pool with (a) three return-jets and (b) two return-jets at $t = 13.4$ hours.

of the particles in less than 3 hours while model A (three-jet configuration) flushes the same amount in approximately 8.5 hours. Thus, model B is more efficient in flushing out the particles.

Figure 10 shows the mean residence time of particles flushed as a function of time. For example, after 8 hours of operation (8 hours after the particles were released) the mean residence time of particles flushed was 2.1 hours for model B and 3.3 hours for model A, consistent with the results of Figure 9.

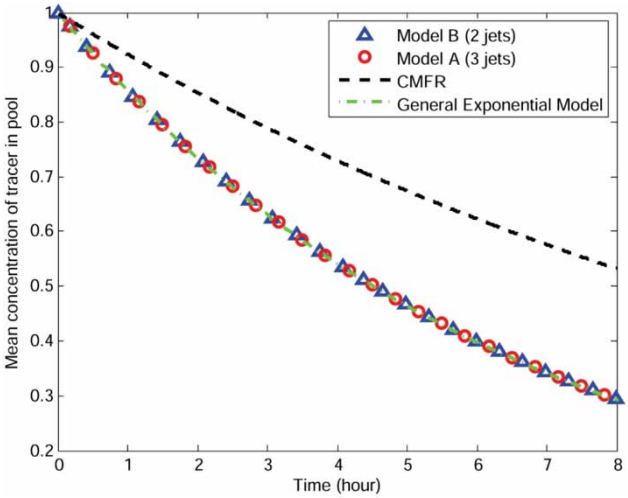

Figure 8 | Time series of mean or volume-averaged tracer residue in the pool with two jets and three jets and corresponding time series based on CMFR and general exponential models.

Figure 11 shows the spatial (local) distributions of particle residence time. Model A (Figure 11(a)) shows long residence times for particles initially released in the center upper right section of the pool, coinciding with the isolated (dead) circulation zone identified earlier through Figure 5(a). Model B (Figure 11(b)) does not exhibit such prominent dead zones as the major re-circulation zones pass through the skimmer and generally have greater speed than in model A (Figure 4), thus local residence times are significantly less.

The previous results reveal that particles behave distinctly from the tracer. In the tracer volume flushing studies, the total tracer within the pool in both models

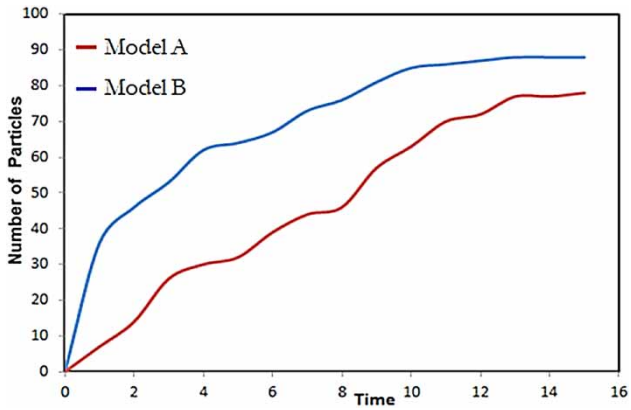

Figure 9 | Number of particles flushed vs. time (hours).

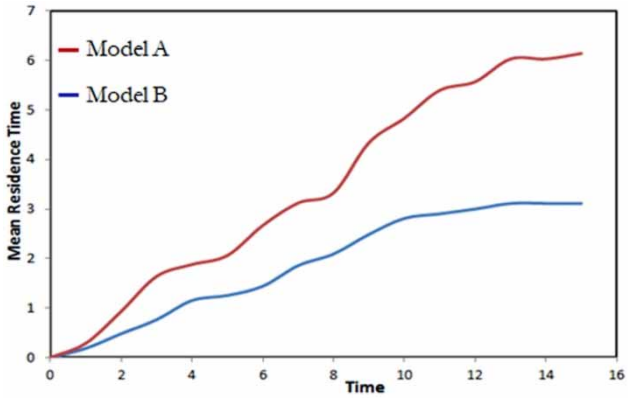

Figure 10 | Mean residence time of particles flushed versus time (hours).

A and B decayed at near identical rates. In contrast, model B was observed to be more efficient at flushing particles. The difference between these Lagrangian and Eulerian results is attributed to the fact that the particles do not exactly follow the motion of the fluid and instead their motion is dictated through Equation (7), whereas the tracer is advected and diffused exactly as the fluid through Equation (5). In the case of the particles, although turbulence diffusion plays a role in establishing the particle path via the random walk model used in Equation (7), results indicate that the mean flow plays a more dominant role in determining the particle path and particle residence time. Thus the particles are more susceptible to stagnation within the recirculation zones of the mean flow than the tracer. Such behavior is consistent with Brennen (2005) who noted that particles are not as strongly affected by turbulence.

Summary of results

In this manuscript, Eulerian and Lagrangian methods were employed to investigate the hydraulic efficiency of

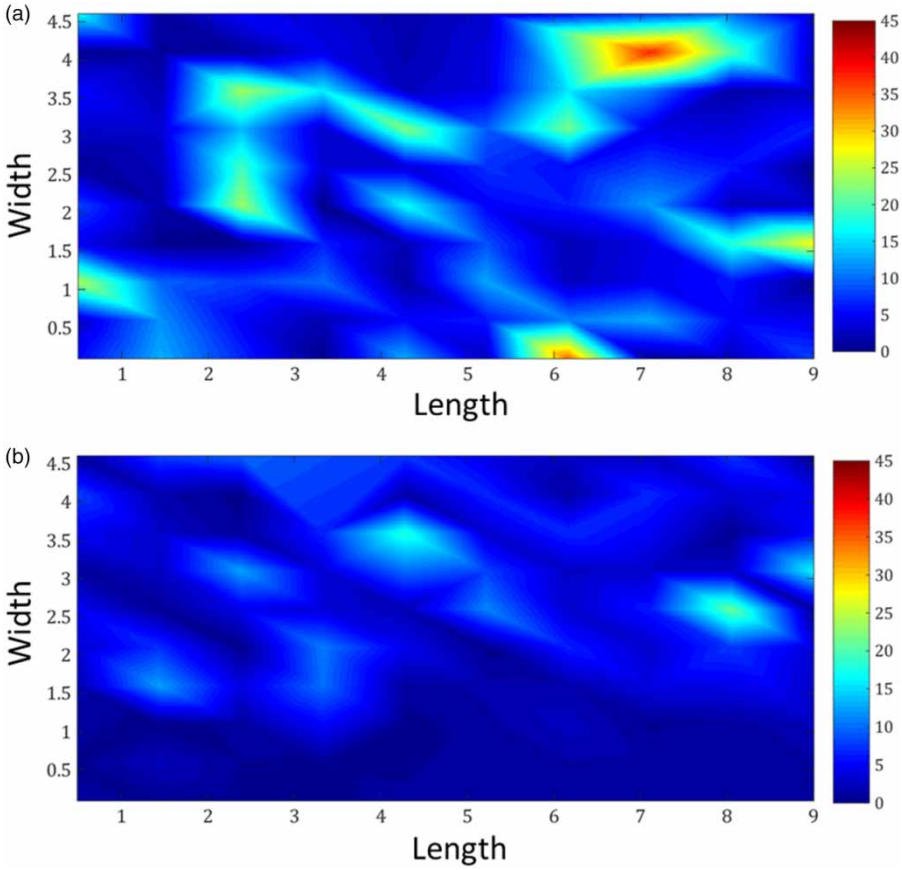

Figure 11 | Spatial RTD (color-coded in hours) based on fluid particles released within a 9 × 4.5 m region on the pool surface in model A (a) and model B (b). Please refer to the online version of this paper to see this figure in color: http://dx.doi.org/10.2166/wh.2018.110.

residential swimming pools. Two return-jet configurations were considered: model A with three jets and model B with two jets. The results from the Eulerian-based tracer pulse studies revealed that advection patterns such as short-circuiting dominate tracer transport within the first hour of tracer release. Turbulent diffusion dominates at later times, but the intensity of the associated turbulent mixing is not sufficient for the pools to be assumed CMFRs throughout their entire operation cycle. This is in contrast to Olympic-sized pools for which the CMFR assumption is applicable (Cloteaux *et al.* 2013) as these pools are characterized by higher flow rates and a greater number of return-jets which promote greater turbulence intensity than in the smaller-scale residential swimming pool cases considered here.

In light of the fact that typical pump operation and associated pool circulation in residential swimming pools is expected to be on cycles on the order of 8 hours long, the filtration efficiency of models A and B over an operation cycle is nearly the same, as predicted by the tracer studies. However, the results from particle tracking show that model B performs better than model A in removing particles, which can be considered representative of bacteria. The difference in pool hydraulic efficiency obtained with tracer and particles is attributed to particles adhering closer to mean flow path-lines, whereas the tracer is more susceptible to mixing caused by turbulence. In the case of model B, the close proximity of re-circulation zones to the skimmer induced by the return-jet configuration coupled with the faster mean speeds along the fluid path-lines lead to significantly shorter particle residence times relative to model A.

FUTURE PERSPECTIVE

The present study has demonstrated the feasibility of the CFD approach as an evaluation and design tool that can help builders design pools characterized by reduced dead zone regions resulting in increased hydraulic efficiency. The current design standards of swimming pools assume perfectly mixed flow (no dead zones), such as in a CMFR regardless of jet/skimmer/drain configuration. However, this assumption may lead to incorrect prediction of removal efficiency of chemicals and pathogens and consequently result in an unsafe swimming environment.

The particle tracking results suggest that return-jets and associated flow circulation pattern should be considered as key parameters in the design of pathogen-free public and/or residential swimming pools. Dead zones or re-circulation zones in the pool are conducive to the formation of biofilms which allow for the collection of harmful bacteria. The particle tracking results suggest that it should be possible to use the return-jet configuration to help minimize the dead zones and thus reduce biofilm formation. Biofilms are the result of cumulative aggregates (comprised of suspended particles, organic matter and microbes) that tend to settle onto surfaces over which the water is slow moving or stagnant (Taylor 2017). The return-jet configuration can be designed to generate sufficiently high turbulence levels throughout the pool to disrupt the formation of the aggregates. Additionally, the return-jet configuration may be designed to generate high water circulation in the pool leading to sufficiently strong shear at the walls to prevent biofilm formation at the walls. This effect should be similar to wall brushing which is a typical maintenance approach. To the knowledge of the authors, no study exists exploring the mechanisms above for preventing or removing biofilm and this should be considered in future research.

The impact of particle size on residence time should also be investigated because pathogens (e.g. bacteria, protozoa, hepatitis A and noroviruses) in swimming pools having varying size.

The current tracer transport simulations were performed with a passive tracer. In future studies, models for chemical reactions and biological inactivation should be included in the governing equations in order to simulate the disinfection process in pools. Guidance for this can be taken from previous CFD analysis applied to ozone and UV disinfection in drinking water treatment systems (e.g. Zhang *et al.* 2014a; Wols *et al.* 2015).

ACKNOWLEDGEMENTS

This research was supported through a grant from Crystal Blue Vortex, LLC and a matching grant from the Florida High Tech Corridor program.

REFERENCES

Beech, J. A., Diaz, R., Ordaz, C. & Palomeque, B. 1980 Nitrates, chlorates and trihalomethanes in swimming pool water. *Am. J. Public Health* **79** (1), 79–82.

Brennen, C. E. 2005 *Fundamentals of Multiphase Flow*. Cambridge University Press, Cambridge.

Caro, J. & Gallego, M. 2007 Assessment of exposure of workers and swimmers to trihalomethanes in an indoor swimming pool. *Environ. Sci. Technol.* **41** (3), 4793–4798.

Cloteaux, A., Gérardin, F. & Midoux, N. 2013 Influence of swimming pool design on hydraulic behavior: a numerical and experimental study. *Engineering* **5** (5), 511.

Cockx, A., Do-quang, Z., Line, A. & Roustan, M. 1999 Use of computational fluid dynamics for simulating hydrodynamics and mass transfer in industrial ozonation towers. *Chem. Eng. Sci.* **54** (21), 5085–5090.

Do-Quang, Z., Cockx, A., Line, A. & Roustan, M. 1999 Computational fluid dynamics applied to water and wastewater treatment facility modeling. *Environ. Eng. Poll.* **1**, 137–147.

Fluent user's guide version 6.3 2006 *Fluent Inc., Lebanon, N.H.* Available from: www.sharcnet.ca/Software/Fluent6/html/ug/node1.htm.

Henry, D. J. & Freeman, E. M. 1995 Finite element analysis and T-10 optimization of ozone contactors. *Ozone Sci. Eng.* **17** (6), 587–606.

Huang, T., Brouckaert, C. J., Docrat, M. & Pryor, M. 2002 A computational fluid dynamics and experimental study of an ozone contactor. *Water Sci. Eng.* **46** (9), 87–93.

Huang, T., Brouckaert, C. J., Pryor, M. & Buckley, C. A. 2004 Application of computational fluid dynamics modeling to an ozone contactor. *Water SA* **30** (1), 51–56.

Launder, B. E. 1978 Heat and mass transport. In: *Turbulence*, Chapter 6 (P. Bradshaw, ed.). Springer, Berlin.

Launder, B. E. & Spalding, D. B. 1974 The numerical computation of turbulent flows. *Comput. Meth. Appl. Mech. Eng.* **3**, 269–289.

Lewis, L., Chew, J., Woodley, I., Colbourne, J. & Pond, K. 2015 The application of computational fluid dynamics and small-scale physical models to assess the effects of operational practices on the risk to public health within large indoor swimming pools. *J. Water Health* **13** (4), 939–952.

Michalski, R. & Mathews, B. 2007 Occurrence of chlorite, chlorate and bromate in disinfected swimming pool water. *Pol. J. Environ. Stud.* **16** (2), 237–241.

Morsi, S. A. & Alexander, A. J. 1972 An investigation of particle trajectories in two-phase flow systems. *J. Fluid Mech.* **55** (2), 193–208.

Pool Water Treatment Advisory Group (PWTAG) 2009 *Swimming Pool Water – Treatment and Quality Standards for Pools and Spas*, 2nd edn. Pool Water Treatment Advisory Group, London.

Taylor, N. 2015 San Juan pool goes drainless. *Pool and Spa News* July 1, 2015.

Taylor, C. 2017 *Water care basics to prevent biofilm formation*. Pool & Spa Marketing September 13, 2017.

Wilcox, D. C. 1994 *Turbulence Modeling for CFD*. DCW Industries, Inc., California.

Wols, B. A., Harmsen, D. J. H., Wanders-Dijk, J., Beerendonk, E. F. & Hofman-Caris, C. H. M. 2015 Degradation of pharmaceuticals in UV (LP)/H 2 O 2 reactors simulated by means of kinetic modeling and computational fluid dynamics (CFD). *Water Res.* **75**, 11–24.

Zhang, J. P., Huck, M., Anderson, B. W. & Stubley, D. G. 2007 A computational fluid dynamics based integrated disinfection design approach for improvement of full-scale ozone contactor performance. *Ozone Sci. Eng. J. Int. Ozone Assoc.* **29** (6), 451–460.

Zhang, J., Tejada-Martínez, A. E. & Zhang, Q. 2013 Hydraulic efficiency in RANS of the flow in a multi-chambered contactor. *J. Hydr. Eng.* **139** (11), 1150–1157.

Zhang, J., Tejada-Martínez, A. E., Zhang, Q. & Lei, H. 2014a Evaluating hydraulic and disinfection efficiencies of a full-scale ozone contactor using a RANS-based modeling framework. *Water Res.* **52**, 155–167.

Zhang, J., Tejada-Martínez, A. E. & Zhang, Q. 2014b Developments in computational fluid dynamics-based modeling framework for disinfection technologies in last recent two decades: a review. *Environ. Softw. Model.* **58**, 71–85.

Zhang, J., Tejada-Martínez, A. E., Zhang, Q. & Lei, H. 2016 Indicators for technological, environmental and economic sustainability of ozone contactors. *Water Res.* **101**, 606–616.

Zwiener, C., Richardson, S. D., De Marini, D. M., Grummt, T., Glauner, T. & Frimmel, F. H. 2007 Drowning in disinfection byproducts? Assessing swimming pool water. *Environ. Sci. Technol.* **41** (2), 363–372.

First received 5 May 2017; accepted in revised form 28 May 2018. Available online 26 June 2018